Derna Academy Journal for Applied Sciences

E-ISSN: 3006-3159

DAJAS

Elemental Geochemistry of the Upper Cretaceous Rakb Formation in Well C3-65, Sarir Field, Sirte Basin, NE Libya

Osama Rahil Shaltami[1,2], Husam Uldin Hamid Alghamari[3], Mustafa A. Ben Hkoma[2,4]

[1]Department of Earth Sciences, Faculty of Science, Benghazi University, Libya
[2]Libyan Centre for Sustainable Development Researches
[3]Arabian Gulf Oil Company (AGOCO), Libya
[4]Libyan Centre for Studies and Researches of Sciences and Environment Technology, Middle Zone Branch, Zliten, Libya

*Corresponding author: E-mail addresses: osama.rahil@yahoo.com

Volume: 4 **Issue: 1** **Page Number: 64 - 84**

Keywords:
Elemental Geochemistry, Rakb Formation, Sarir Field, Sirte Basin, Libya

Received: 27\07\2025
Accepted: 07\08\2025
Published: 08\08\2025
DOI:
https://doi.org/10.71147/mmpnge43

ABSTRACT

Assessing the elemental geochemistry of the Rakb Formation in well C3-65, Sarir Field, Sirte Basin, was the goal of this work. The results demonstrated that the Rakb Formation is classified as silica-rich argillaceous shale as indicated by the content of quartz and clay minerals. Numerous sources contribute to the Rakb Formation, including igneous (mafic, intermediate, and felsic rocks) and sedimentary (quartzose rocks), as showed by the plots of Al_2O_3 versus TiO_2, SiO_2 versus FeO, CaO versus Na_2O, F1 versus F2, and SiO_2/10-CaO-MgO-Na_2O+K_2O. Several parameters, including Fe/Al, Mn*, and SO_3, suggested that the Rakb Formation's proven depositional setting is the shallow anoxic marine environment. The plots of MgO versus Fe_2O_3, Al_2O_3 versus P_2O_5, Ca versus Fe, and CaO versus MgO supported this assumption. There was clear terrestrial input during deposition as indicated by the Ti/Al and Al/(Al+Fe) ratios. The Rakb Formation is considered part of the coastal facies as presented by the plot of Al_2O_3/(Al_2O_3+Fe_2O_3) versus Fe_2O_3/TiO_2. The Rakb Formation is not significantly affected by severe diagenesis as confirmed by the plots of CaO/Al_2O_3 versus P_2O_5/Al_2O_3. According to the paleoweathering indices (RR, CIA, CIW, PIA, and CIW′), the source area experienced moderate to high levels of paleoweathering intensity. Conditions during deposition were mostly semi-arid to semi-humid, as verified by the CIA, K_2O/Al_2O_3, and T values. The studied sediments are obviously immature, based on the ICV values. Paleoproductivity fluctuated from low to high as displayed by the P/Al and P/Ti ratios. Th plots of Al_2O_3/(100-SiO_2) versus Fe_2O_3/(100-SiO_2), SiO_2 versus K_2O/Na_2O, and SiO_2/20-K_2O+Na_2O-TiO_2+Fe_2O_3+MgO confirmed that he paleotectonic environment of the Rakb Formation is the continental margin.

1. INTRODUCTION

One of the many sedimentary basins in Libya is the Sirte Basin. The basin stretches southward from the Gulf of Sirte in central Libya. This basin is thought to be the most recent of all the Libyan basins.

The Sirte Basin may have formed as a result of the collapse of the Sirte Arch during the Mesozoic Era (Late Jurassic to Early Cretaceous) (Hallett, 2002). The stratigraphic chart is depicted in Fig. 1. Numerous wells have been drilled in the Sirte Basin, providing information on the thickness, facies, and extent of the various formations. They also show which units serve as effective source rocks, cap rocks, and reservoirs. The Sirte Basin contains 33 trillion cubic feet of gas and 45 billion barrels of oil, making it Libya's largest conventional hydrocarbon reserve (Hallett and Clark-Lowes, 2016). There is also a substantial unconventional hydrocarbon reserve in the basin. The reserves of shale oil and shale gas are 456.4 billion barrels and 647.7 trillion cubic feet, respectively (EIA, 2015). A characteristic horizon between the Rachmat and Sirte formations in the eastern Sirte Basin was dubbed the Rakb Formation by Williams (1972) and referred to as the Tagrifat Formation by Barr and Weegar (1972). The well Nl-59, which is situated on the Amal Shelf next to the Awjilah field, is where the type section was identified. In the type section the formation consists of 91 m of calcarenite and calcareous shale (Williams, 1972). The possible age of the Rakb Formation is the Late Cretaceous. The formation is only found in the eastern Sirte Basin (between Awjilah area and Harash field, Williams, 1972). In the Awjilah and Nafoora fields, the formation serves as a major oil reservoir. It most likely has some potential as a local oil source (Hallett, 2002). The confirmed depositional setting for the Rakb Formation is the shallow marine environment (Williams, 1972). In other areas, it is most likely comparable to the lower Sirte Formation (Hallett, 2002). In this work the geochemical characteristics of the Rakb Formation in well C3-65 (Fig. 2), Sarir Field, Sirte Basin, were described. British Petroleum (BP) drilled the well under study in 1961, and it is owned by the Arabian Gulf Oil Company (AGOCO) in Libya. This study relied on the concentration of the major oxides. The following was ascertained: (1) Classification; (2) Provenance; (3) Depositional environment; (4) Diagenesis; (5) Paleoweathering; (6) Paleoclimate; (7) Maturity; (8) Paleoproductivity; and (9) Paleotectonic setting. After reviewing the publications, it became clear that this work would be the first study on the elemental geochemistry of the Rakb Formation. All previous geochemical studies focused on organic geochemistry (e.g., Aboglila et al., 2011; Aboglila and Elkhalgi, 2013).

2. METHOD

The core samples from Arabian Gulf Oil Company (AGOCO) was used in this work. The following is the work plan:

(1) Thirteen core shale samples, ranging in depth from 7750 to 8622 ft, were chosen from well C3-65.

(2) To remove impurities, distilled water was used to clean the samples.

(3) The samples were dried at 100°C for 5 hours.

(4) The samples were ground using a vibrating mill. The grinding process took approximately 2 minutes.

(5) Ten grams of the samples were taken and they were ground again to a powder size of 0.5 to 100 μm with the addition of grinding aid.

(6) The major oxide data were obtained by inserting the samples into an X-ray fluorescence (XRF) instrument after they had been compressed in a press. It took around five minutes to complete the chemical analysis. This analysis was performed in the Laboratory of Al-Fattaih Cement Factory, Darnah, Libya.

3. ETHIC APPROVAL

This paper is part of the master's thesis of Husam Uldin Hamid Alghamari (second author), who obtained permission from the Arabian Gulf Oil Company (AGOCO) to analyze the samples and use them in his work.

4. RESULT

Table 1 contains the data gathered using the XRF technique. The concentration of FeO was determined using the following equation: FeO = 0.8998*Fe2O3.

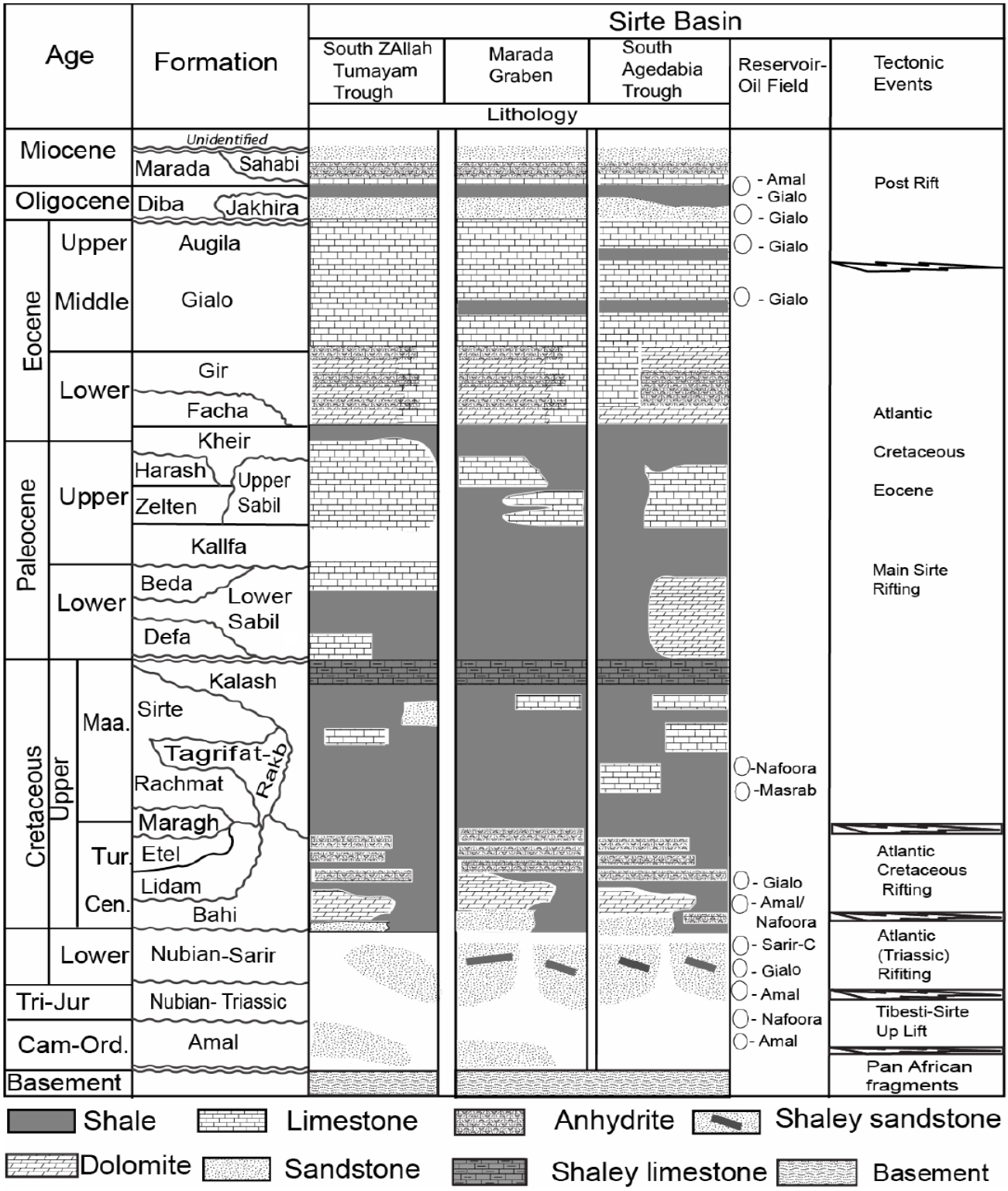

Fig. 1: Stratigraphic column of the Sirte Basin (drawn by Barr and Weeger, 1972 and modified by Aboglila *et al.,* 2010).

5. DISCUSSION

5.1. CLASSIFICATION

In addition to the commonly used geochemical sand-shale classification diagram of log(SiO2/Al2O3) versus log(Fe2O3/K2O) (Herron, 1988); the SiO2-Al2O3+Fe2O3-CaO+MgO diagram (Hasterok et al., 2018) is another attempt to differentiate sedimentary rocks. These two diagrams indicate that the studied samples are mainly classified as shale (Figs. 3 and 4). The binary plot of Na2O versus K2O (Fig. 5) illustrates that the studied samples contain medium to high quartz content, which explains why some of the samples are present in the sandstone field in Fig. 3.

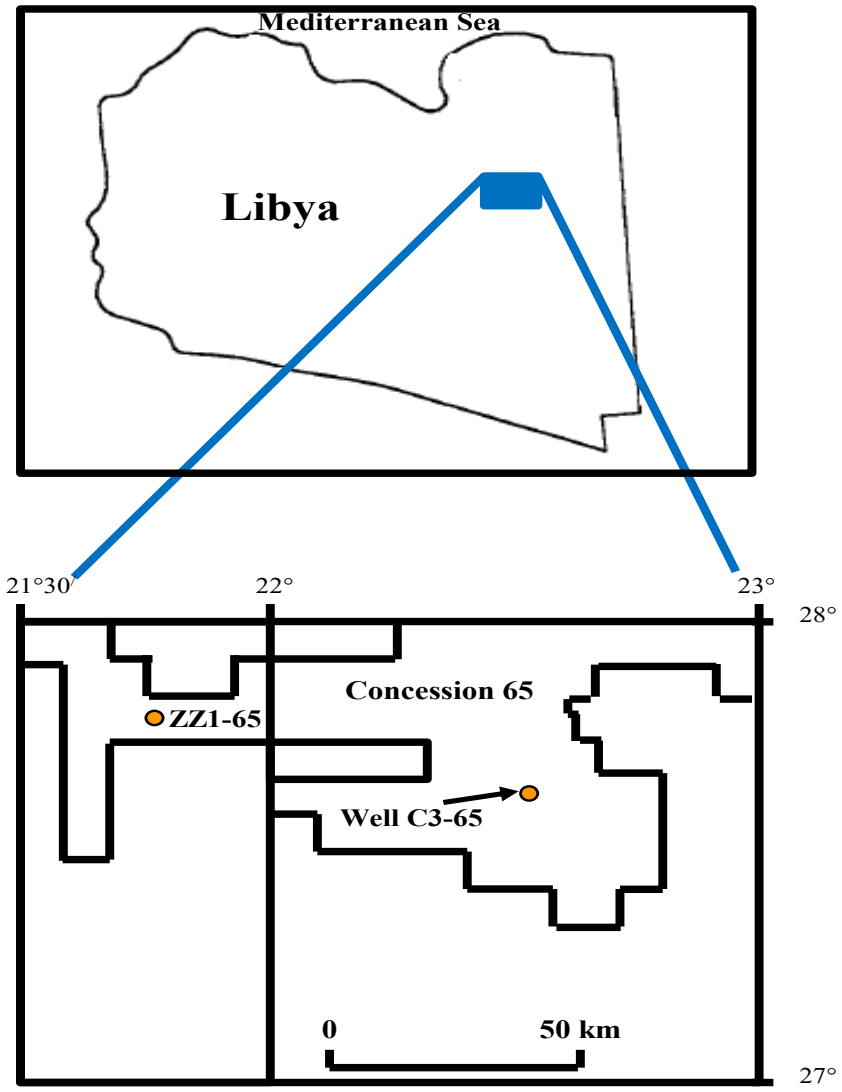

Fig. 2: Location map of the studied well (modified after El-Mehdawi, 1998).

Table 1: Chemical analysis data (major oxides in wt%) of the Rakb Formation in well C3-65

Sample No.	Depth (ft)	SiO_2	TiO_2	Al_2O_3	Fe_2O_3	FeO*	MnO	MgO	CaO	K_2O	Na_2O	Cl	SO_3	P_2O_5
R1	7750	56.46	0.58	13.77	5.93	5.34	0.01	4.15	16.89	0.90	1.04	0.10	0.19	0.21
R2	7755	80.93	0.67	14.70	6.08	5.47	0.01	4.45	14.78	1.02	1.20	0.11	0.24	0.36
R3	7800	57.45	1.63	20.53	8.07	7.26	0.01	6.55	4.58	0.80	1.40	0.27	0.19	0.11
R4	8410	70.24	1.43	18.11	7.55	6.79	0.01	4.96	4.66	1.35	2.10	0.24	0.08	0.12
R5	8425	70.77	1.59	18.08	8.16	7.34	0.02	5.03	4.60	1.38	2.00	0.25	0.12	0.13
R6	8443	78.38	1.26	14.04	8.00	7.20	0.02	3.00	5.78	1.07	1.61	0.26	0.17	0.14
R7	8463	68.16	1.66	17.41	11.54	10.38	0.13	4.85	4.81	1.27	1.82	0.22	0.08	0.14
R8	8487	63.43	1.79	18.48	7.80	7.02	0.01	5.38	4.65	1.38	1.69	0.30	0.18	0.10
R9	8515	66.26	0.74	11.30	7.24	6.51	0.02	1.67	10.12	1.00	0.80	0.16	0.05	0.16
R10	8565	66.33	1.62	17.11	7.03	6.33	0.02	4.53	6.19	1.31	1.95	0.20	0.06	0.11
R11	8588	70.74	1.69	17.60	6.27	5.64	0.001	4.72	4.70	3.00	1.61	0.22	0.12	0.12
R12	8601	44.36	0.60	9.30	5.30	4.77	0.01	2.28	14.97	1.59	1.11	0.09	1.80	0.16
R13	8622	59.97	0.87	12.34	5.93	5.34	0.01	2.93	11.05	2.53	1.26	0.13	0.89	0.14

The SiO_2/Al_2O_3 ratio was proposed by Pettijohn (1975) as a suitable stand-in for grain size. When the SiO_2/Al_2O_3 ratio ≥3.9, this indicates that the mud rocks are of the sandy type (sandy mud, Saadawi et al., 2023). The SiO_2/Al_2O_3 ratio in the Rakb Formation ranges from 2.8 to 5.86. The SiO_2/Al_2O_3 ratio in the studied samples ≥ 3.9 (except for samples R3 and R8), indicating that they belong to the sandy type. This also explains the presence of some samples in the sandstone field in Fig. 3.

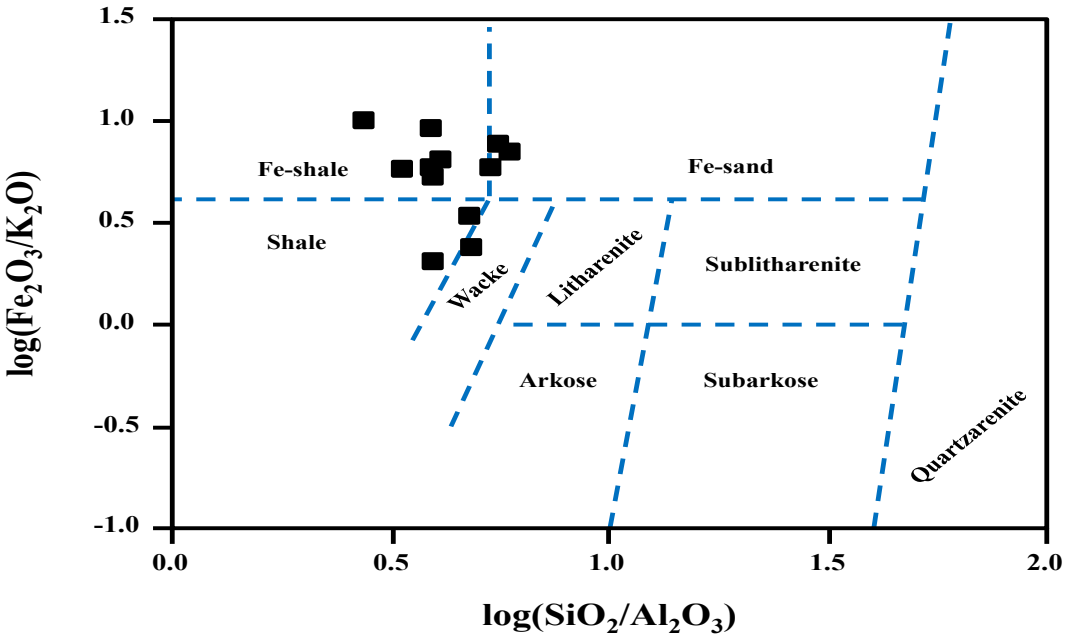

Fig. 3: Binary plot of $\log(SiO_2/Al_2O_3)$ vs. $\log(Fe_2O_3/K_2O)$ showing the classification of the studied samples (fields after Herron, 1988).

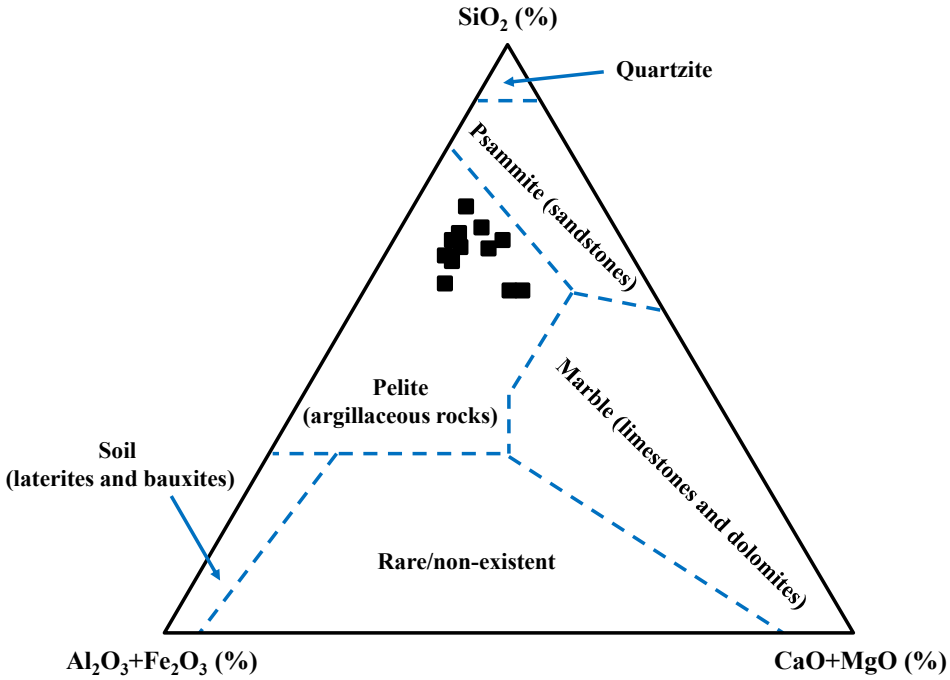

Fig. 4: Ternary plot of SiO_2-Al_2O_3+Fe_2O_3-CaO+MgO showing the classification of the studied samples (fields after Hasterok *et al.,* 2018).

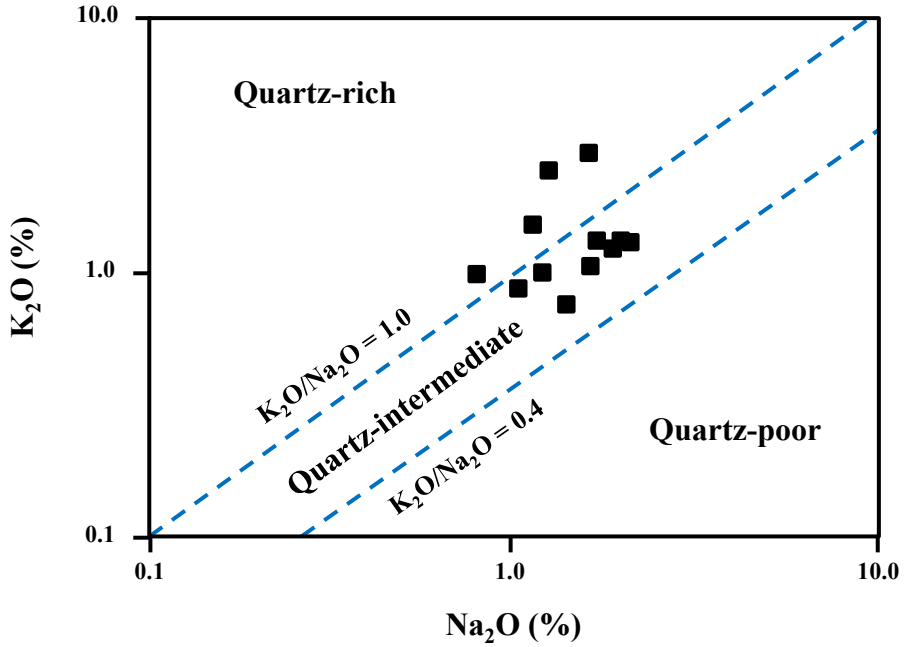

Fig. 5: Binary plot of Na_2O vs. K_2O showing the abundance of quartz in the Rakb Formation (fields after Crook, 1974).

The quartz content in the studied samples ranges from medium to high (as mentioned previously) in addition to the high clay mineral content as shown in the binary plots of Al_2O_3 versus FeO (Fig. 6) and $(Na_2O+K_2O)/(Al_2O_3+Na_2O+K_2O)$ versus $(SiO_2+Na_2O+K_2O)/(SiO_2+Al_2O_3+Na_2O+K_2O)$ (Fig. 7), which indicates that the studied samples are classified as silica-rich argillaceous shale based on the classification of Gamero-Diaz *et al.,* (2012).

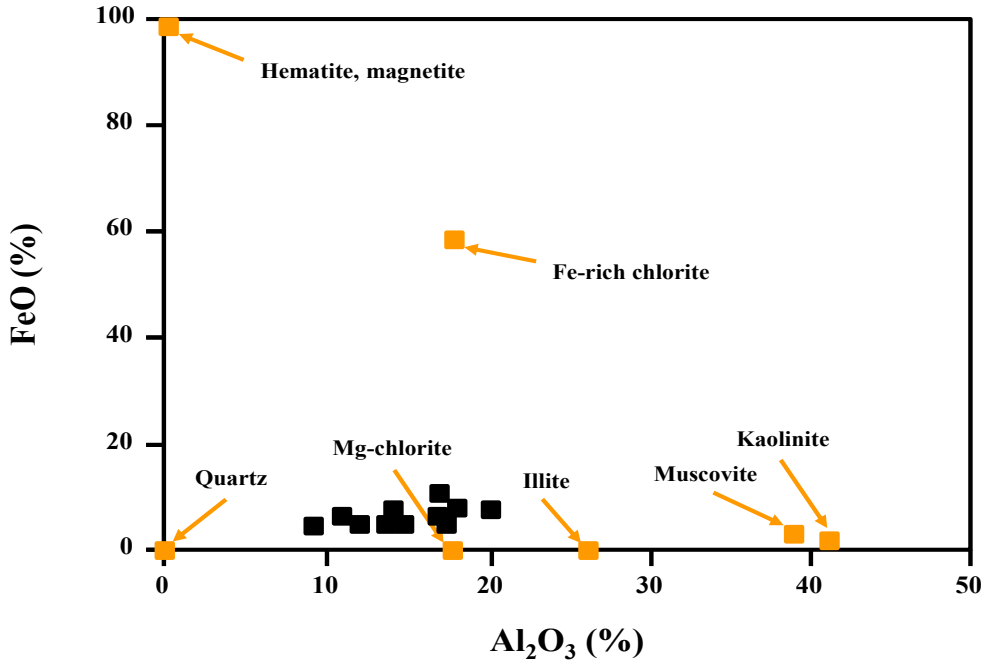

Fig. 6: Binary plot of Al_2O_3 vs. FeO showing the clay mineral richness in the studied shales (fields after Cullers and Podkovyrov, 2000).

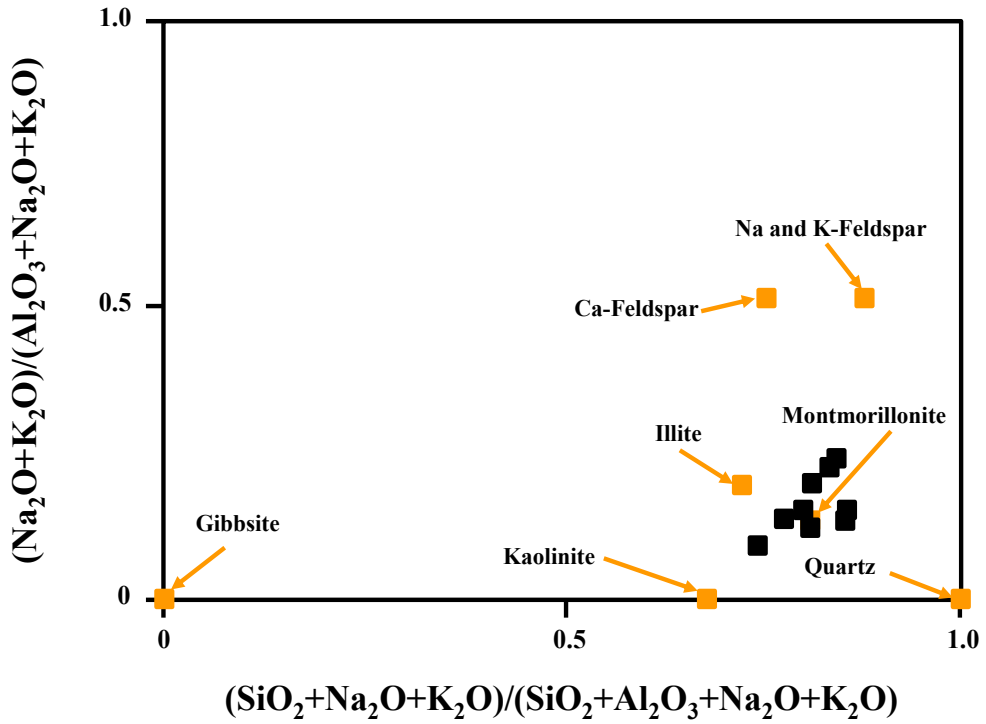

Fig. 7: Binary plot of $(Na_2O+K_2O)/(Al_2O_3+Na_2O+K_2O)$ vs. $(SiO_2+Na_2O+K_2O)/(SiO_2+Al_2O_3+Na_2O+K_2O)$ showing the clay mineral richness in the studied shales (fields after Kronberg and Nesbitt, 1981).

5.2. PROVENANCE

In felsic, intermediate, and mafic rocks, the Al_2O_3/TiO_2 ratios clearly differ (21-70, 8-21, and 3-8, respectively, Hayashi *et al.,* 1997). The clear fluctuation in the Al_2O_3/TiO_2 ratio (10.32-23.74) suggests mixed sources of the Rakb Formation. The plots of Al_2O_3 versus TiO_2 (Fig. 8), SiO_2 versus FeO (Fig. 9), CaO versus Na_2O (Fig. 10), discriminant function 1 (F1) versus discriminant function 2 (F2) (Fig. 11), and $SiO_2/10$-CaO-MgO-Na_2O+K_2O (Fig. 12) also indicate that there are multiple sources for the Rakb Formation, including igneous (mafic, intermediate and felsic rocks) and sedimentary (quartzose rocks). The following equations are used to compute the discriminant functions:

$$F1 = (-1.773\times TiO_2)+(0.607\times Al_2O_3)+(0.76\times Fe_2O_3)+(-1.5\times MgO)+(0.616\times CaO)+ (0.509\times Na_2O)+(-1.22\times K_2O)+(-9.09)$$

$$F2 = (0.445\times TiO_2)+(0.07\times Al_2O_3)+(-0.25\times Fe_2O_3)+(-1.142\times MgO)+(0.432\times Na_2O)+ (1.426\times K_2O)+(-6.861)$$

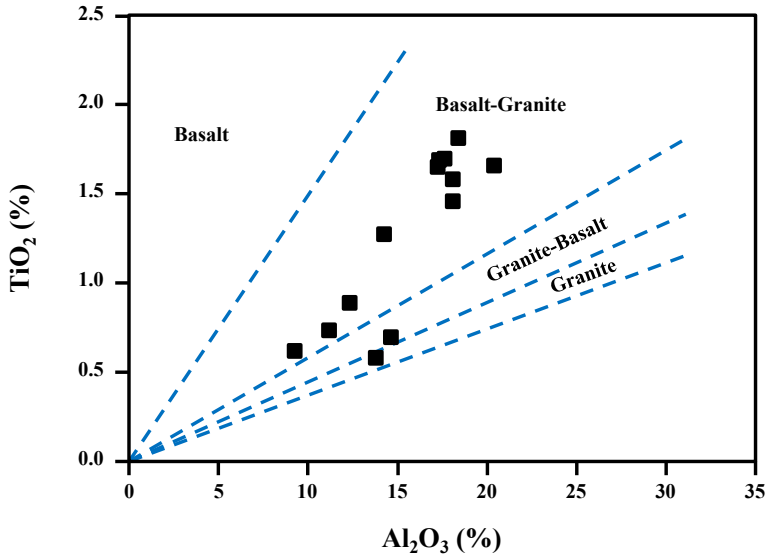

Fig. 8: Binary plot of Al_2O_3 vs. TiO_2 showing the provenance of the Rakb Formation (fields after Hayashi et al., 1997).

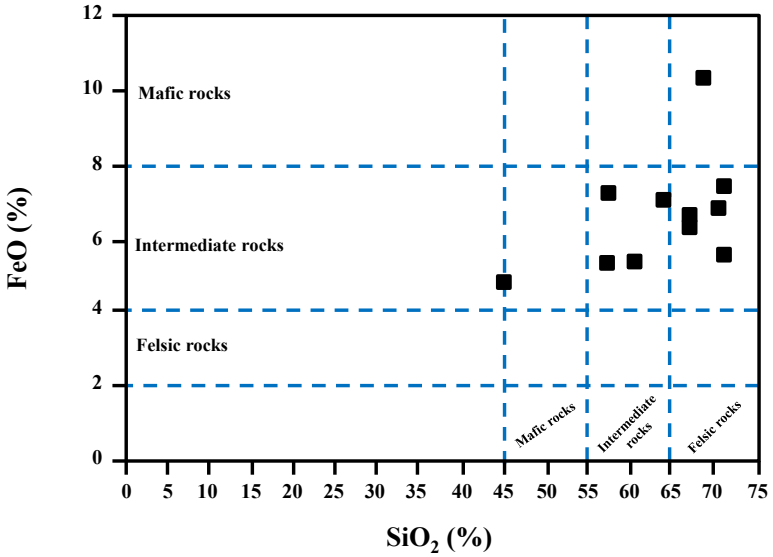

Fig. 9: Binary plot of SiO_2 vs. FeO showing the provenance of the Rakb Formation (fields after Shaltami *et al.,* 2024).

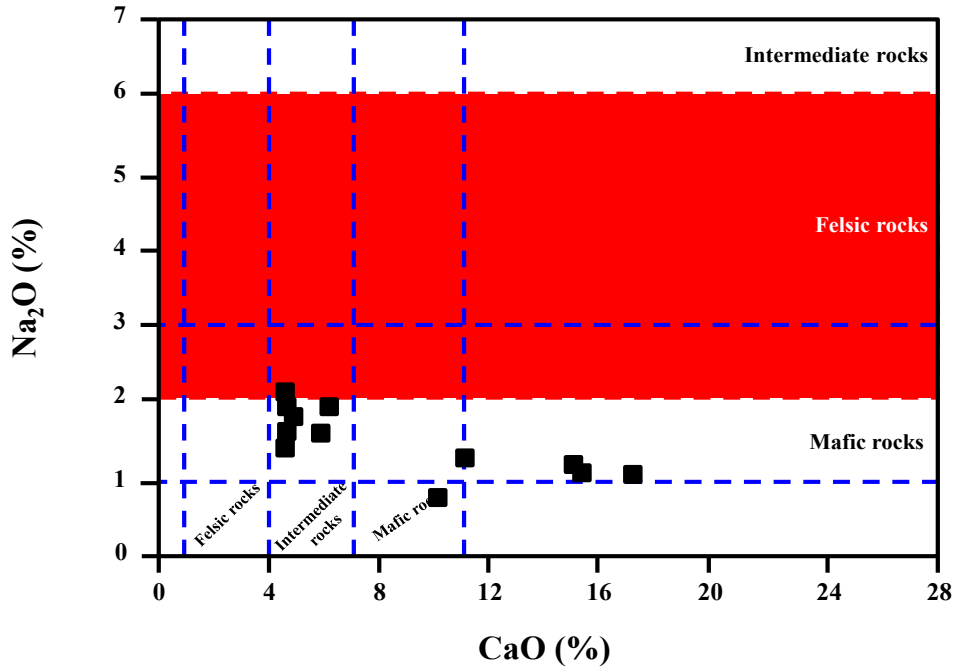

Fig. 10: Binary plot of CaO vs. Na_2O showing the provenance of the Rakb Formation (fields after Shaltami, 2024).

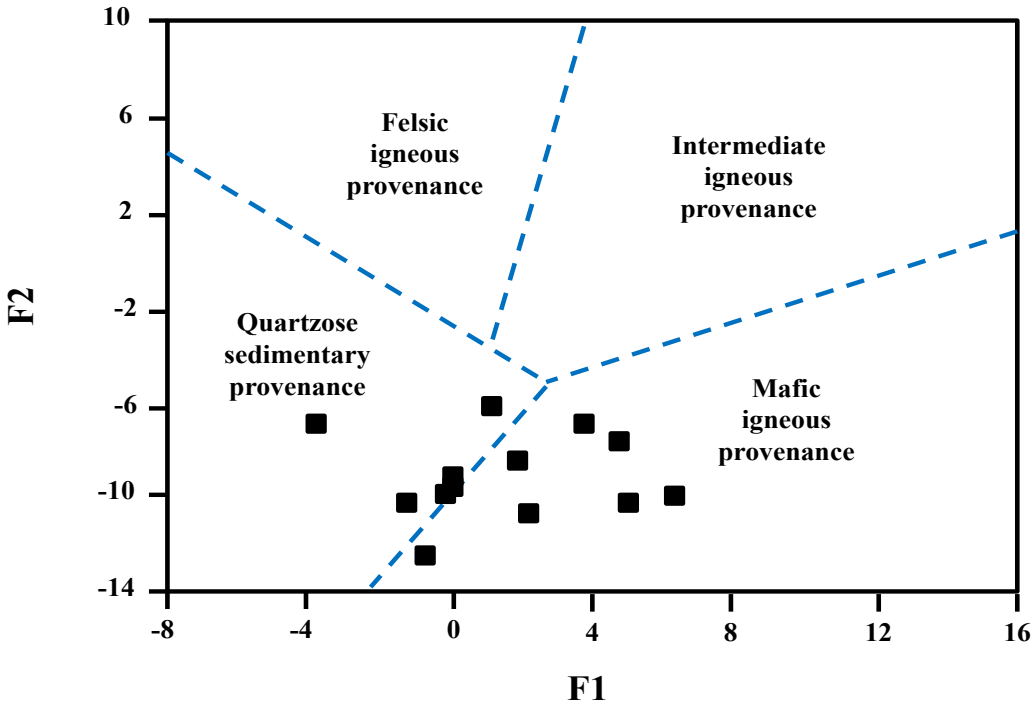

Fig. 11: Binary plot of F1 vs. F2 showing the provenance of the Rakb Formation (fields after Roser and Korsch, 1988).

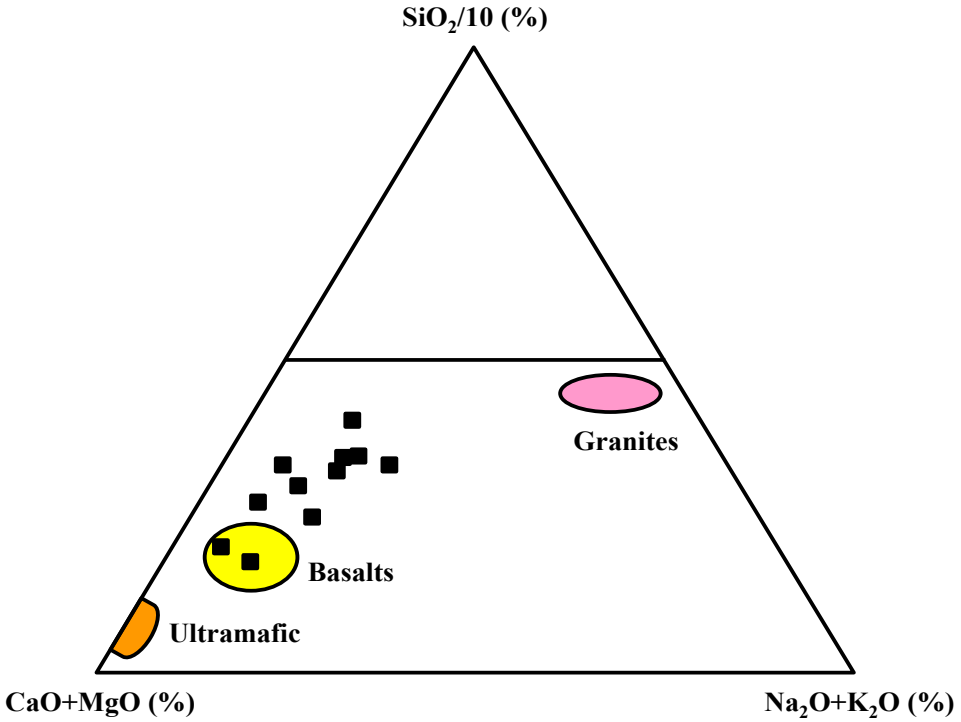

Fig. 12: Ternary of SiO_2/10-CaO-MgO-Na_2O+K_2O showing the provenance of the studied formations (fields after Taylor and McLennan, 1985).

5.3. Depositional Environment

Khan *et al.* (2023) claim that the water depth can be ascertained using the Fe/(Ca+Mg) ratio. Deep water settings are indicated by the high Fe/(Ca+Mg) ratios. According to Murphy *et al.* (2000), the Ti/Al ratio is the most reliable geochemical parameter for estimating the terrestrial source. Low terrestrial input is indicated by low Ti/Al ratios. Furthermore, the terrestrial origin can be assumed if the Al/(Al+Fe) ratio exceeds 0.4 (Liu *et al.,* 2015). The binary plot of MgO versus Fe_2O_3 (Fig. 13) indicates that the confirmed depositional setting for the Rakb Formation is the marine environment. The presence of sample R9 in the field of nonmarine and deltaic can be attributed to the presence of terrestrial input. The Ti/Al and Al/(Al+Fe) ratios (0.05-0.11 and 0.53-0.68, respectively) support this assumption. The water depth can be ascertained using the binary plots of Al_2O_3 versus P_2O_5 (Fig. 14), Ca versus Fe (Fig. 15) and CaO versus MgO (Fig. 16). These discrimination diagrams confirm the deposition of the Rakb Formation in a shallow marine environment. The average content of SO_3 (0.32%) in the Rakb Formation is greater than the values reported by Pettijohn (1975) (0.07-0.10%). The comparatively high content suggests an evaporation medium, supporting the idea that the Rakb Formation was deposited in a shallow marine environment. The low Fe/(Ca+Mg) ratios (0.29-1.28) also suggest deposition in a shallow marine environment. In the binary plot of Al_2O_3/(Al_2O_3+Fe_2O_3) versus Fe_2O_3/TiO_2 (Fig. 17) the Rakb Formation falls in the field of coastal facies.

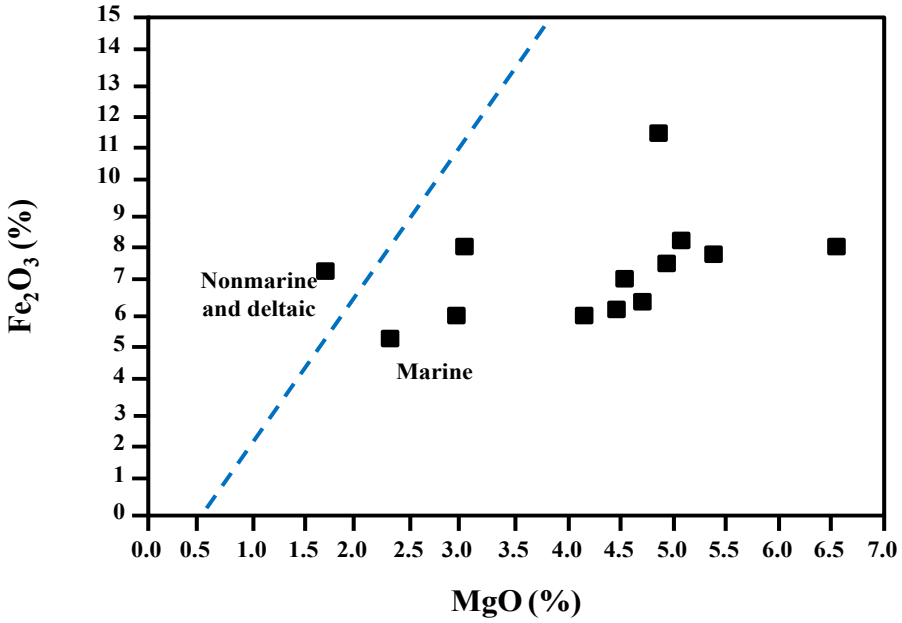

Fig. 13: Binary plot of MgO vs. Fe_2O_3 showing the depositional environment of the Rakb Formation (fields after Ratcliffe *et al.,* 2007).

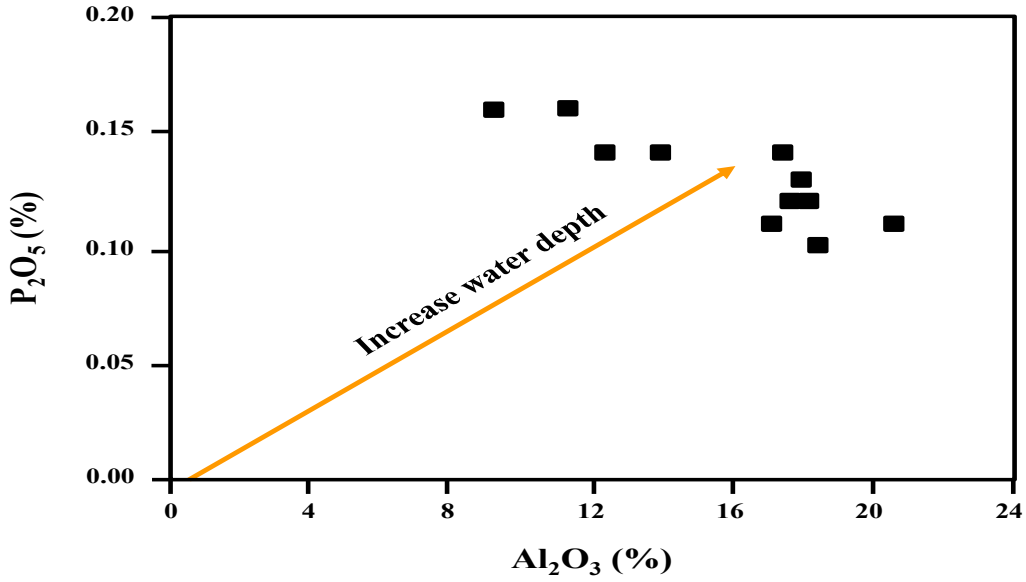

Fig. 14: Binary plot of Al_2O_3 vs. P_2O_5 showing the depositional environment of the Rakb Formation (fields after Dhannoun and Al-Dlemi, 2013).

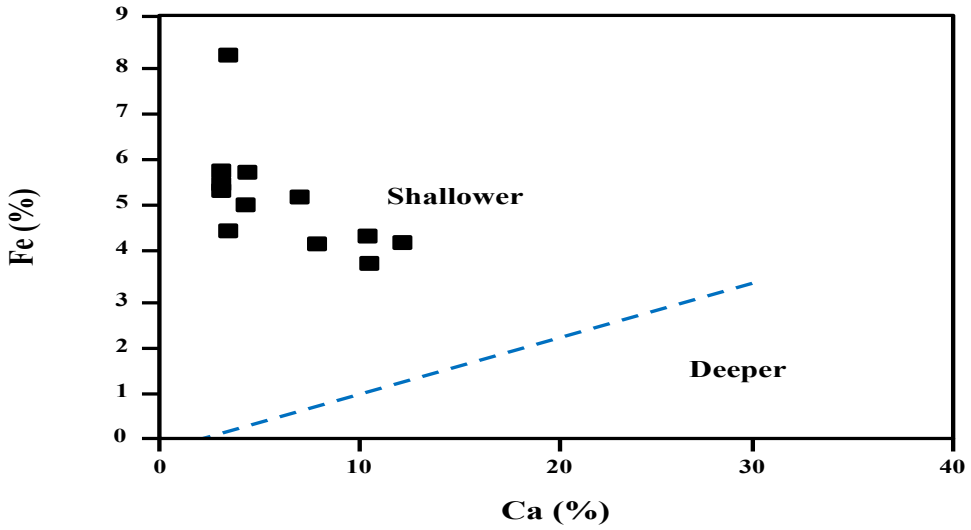

Fig. 15: Binary plot of Ca vs. Fe showing the depositional environment of the Rakb Formation (modified after Naseem *et al.,* 2005).

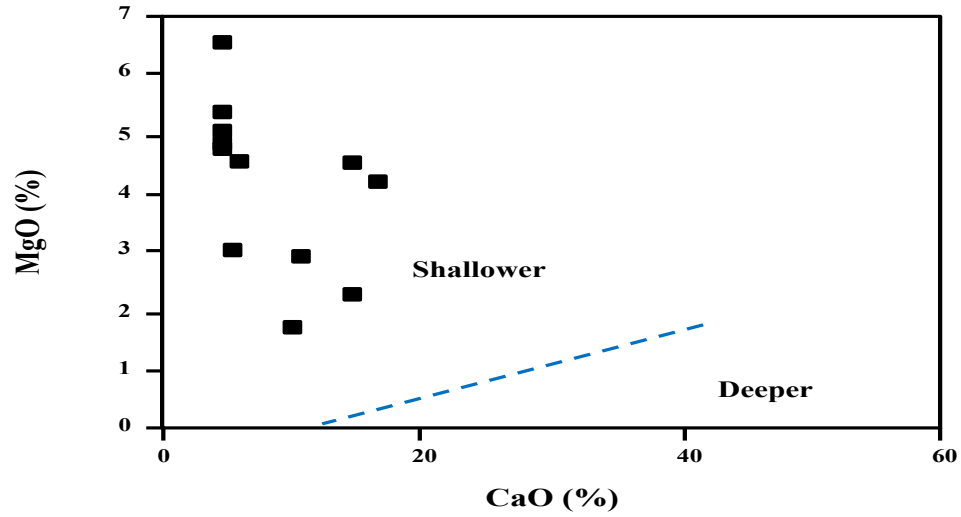

Fig. 16: Binary plot of CaO vs. MgO showing the depositional environment of the Rakb Formation (modified after Naseem *et al.,* 2005)

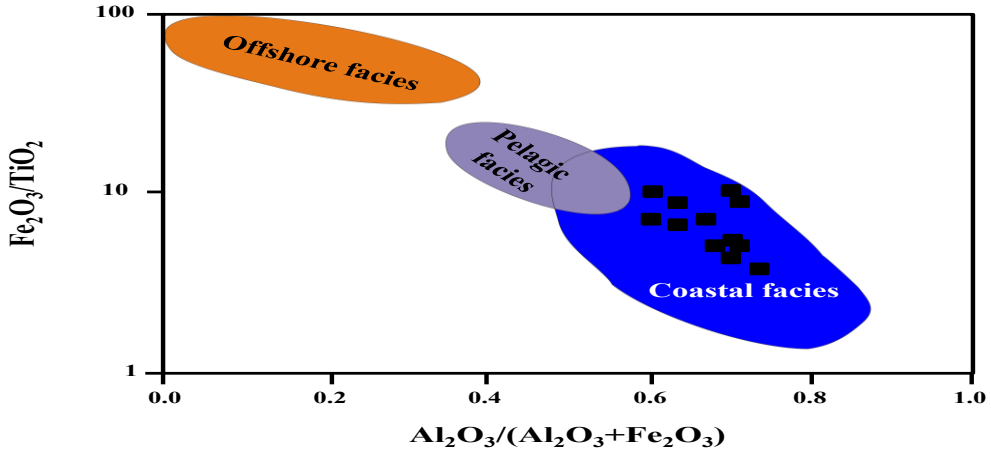

Fig. 17: Binary plot of $Al_2O_3/(Al_2O_3+Fe_2O_3)$ vs. Fe_2O_3/TiO_2 showing the depositional environment of the Rakb Formation (fields after He *et al.,* 2019).

Lyons and Severmann (2006) are of the opinion that high Fe/Al ratios (>0.5-0.6) suggest euxinic conditions. Moreover, positive values of Mn* indicate oxic conditions, while negative values show anoxia (Machhour *et al.,* 1994; Bellanca *et al.,* 1996). Mn* is computed using the following equation: $Mn^* = \log((Mn_{sample}/Mn_{shale})/(Fe_{sample}/Fe_{shale})$, Where, Mn_{shale} = 600 ppm and Fe_{shale} = 46150 ppm (Wedepohl, 1978). The Mn content (0.001-0.13%) suggests that the Rakb Formation was formed in reducing conditions, which causes Mn to leach and lowers its recorded amounts. The values of Fe/Al and Mn* ranges from 0.47 to 0.88 and −1.76 to −0.02, respectively, which also indicates the predominance of anoxic conditions during deposition.

5.4. PALEOWEATHERING

The main paleoweathering indices are Ruxton ratio (RR), chemical index of alteration (CIA), chemical index of weathering (CIW), plagioclase index of alteration (PIA), and modified version of chemical index of weathering (CIW′). These indices are calculated using the following equations:

$$RR = SiO_2/Al_2O_3 \text{ (Ruxton, 1968)}$$
$$CIA = (Al_2O_3/(Al_2O_3+CaO^*+Na_2O+K_2O))100 \text{ (Nesbitt and Young, 1982)}$$
$$CIW = (Al_2O_3/(Al_2O_3+CaO^*+Na_2O))100 \text{ (Harnois, 1988)}$$
$$PIA = ((Al_2O_3-K_2O)/((Al_2O_3-K_2O)+CaO^*+Na_2O))100 \text{ (Fedo } et\ al.,\text{ 1995)}$$
$$CIW' = (Al_2O_3/(Al_2O_3+ Na_2O))100 \text{ (Cullers, 2000)}$$

CaO* indicates the amount of CaO present in the silicate fraction. The concentrations of CaO, P_2O_5, and Na_2O can be used to calculate CaO*. If $Na_2O>CaO-P_2O_5$, then $CaO^* = CaO-P_2O_5$, while if $Na_2O<CaO-P_2O_5$, then $CaO^* = Na_2O$ (McLennan *et al.,* 1993). In the studied samples, the molar ratio of P_2O_5 was found to be greater than the molar ratio of Na_2O when deducted from the molar ratio of CaO. Therefore, the molar proportion of Na_2O is therefore considered to be the molar proportion of CaO*. In the Rakb Formation, the intensity of paleoweathering was moderate to high, according to RR (2.8-5.86), CIA (70.94-85.08%), CIW (80.73-88%), PIA (77.64-87.57%), and CIW′ (89.34-93.62%) values. More support for this assumption can be found in the ternary plot of Al_2O_3-(Na_2O+CaO*)-K_2O (A-CN-K, Fig. 18).

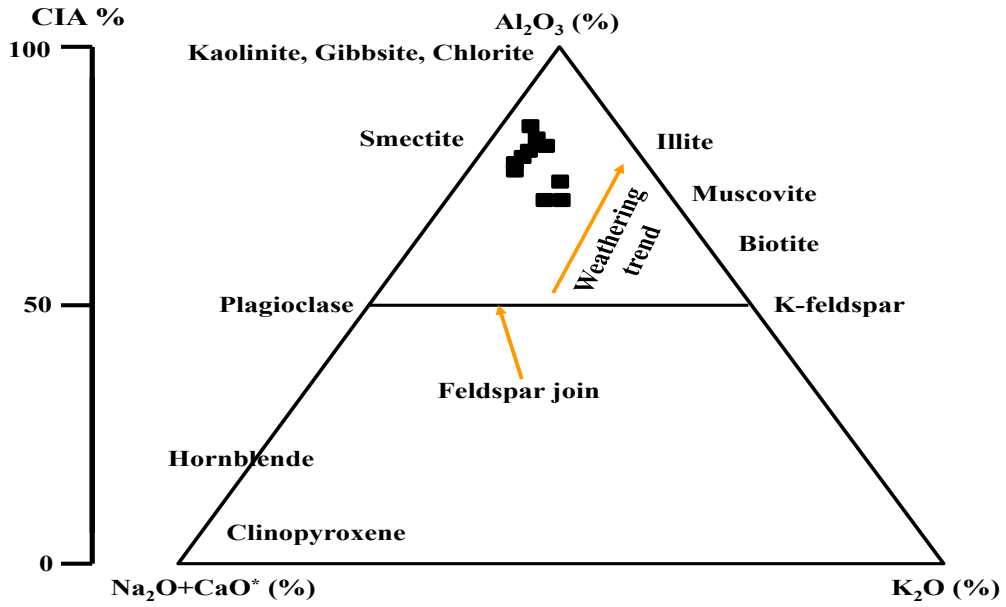

Fig. 18: Ternary plot of A-CN-K showing the paleoweathering intensity in the source area (fields after Nesbitt and Young, 1982).

5.5. DIAGENESIS

The minor impact of the diagenetic changes on the geochemical proxies is confirmed by the binary plots of CaO/Al_2O_3 versus P_2O_5/Al_2O_3 (Fig. 19) and CaO/Al_2O_3 versus Fe_2O_3/Al_2O_3 (Fig. 20). These plots demonstrate that the Rakb Formation is grouped away from the field of severe diagenesis.

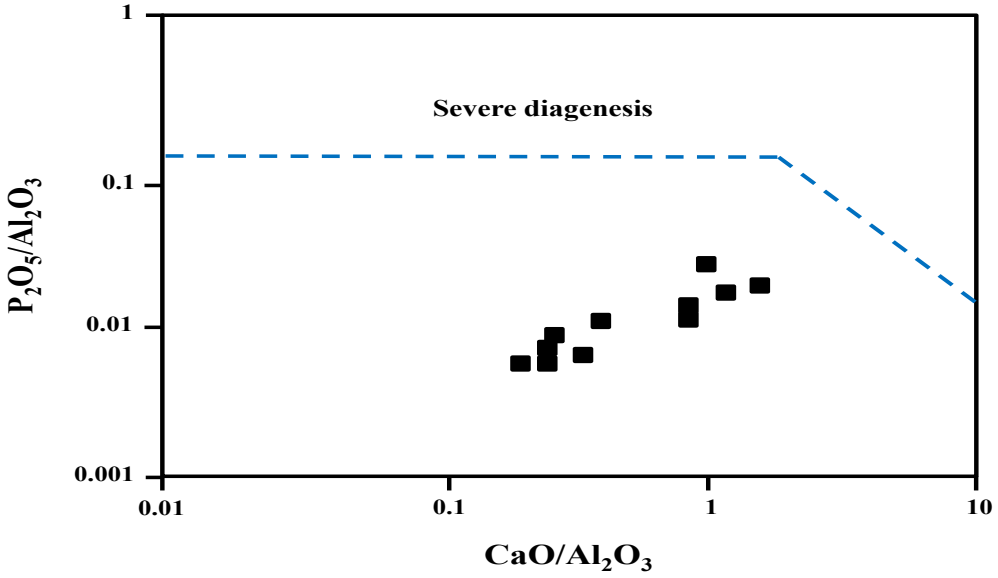

Fig. 19: Binary plot of CaO/Al_2O_3 vs. P_2O_5/Al_2O_3 showing the impact of diagenesis on chemical composition of the Rakb Formation (fields after Ibe and Okon, 2021).

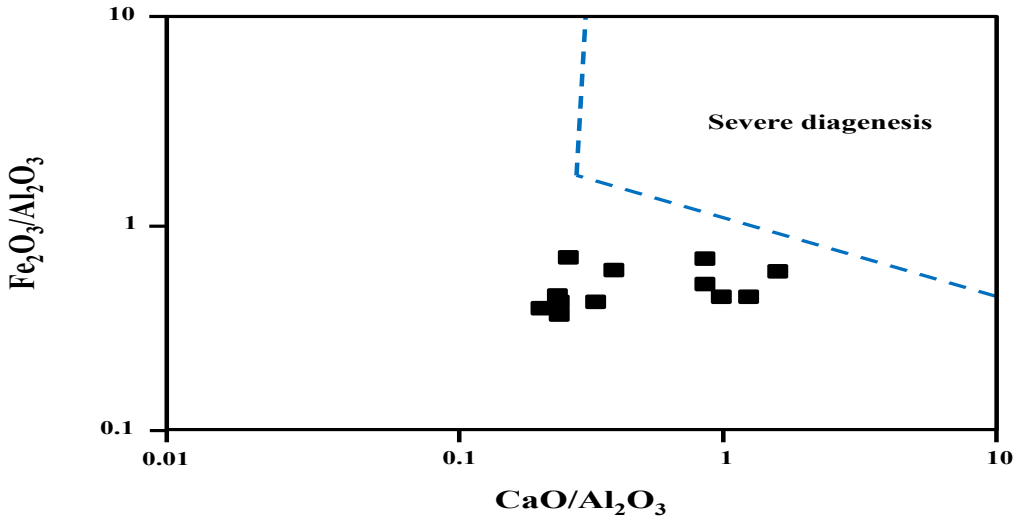

Fig. 20: Binary plot of CaO/Al_2O_3 vs. Fe_2O_3/Al_2O_3 showing the impact of diagenesis on chemical composition of the Rakb Formation (fields after Ibe and Okon, 2021).

5.6. PALEOCLIMATE

Numerous markers, including CIA (Nesbitt and Young, 1982), and K_2O/Al_2O_3 (Roy and Roser, 2013), have been used to ascertain the paleoclimate. Climate can be classified into arid, semi-arid to semi-humid, and humid based on the CIA values (<70%, 70-80%, and 80-100%, respectively) (Nesbitt and Young, 1982). Low K_2O/Al_2O_3 ratios (<0.2) are indicative of humid climate, while arid climate is linked to high K_2O/Al_2O_3 ratios (>0.2, Roy and Roser, 2013). Cao *et al.,* (2019) proposed an equation to calculate the ancient surface temperature based on the CIA values: $T(°C) = 0.56 \times CIA - 25.7$.

The binary plot of $Al_2O_3+K_2O+Na_2O$ versus SiO_2 (Fig. 21) indicates that the Rakb Formation was deposited in arid conditions, while the values of CIA, K_2O/Al_2O_3, and T (70.94-85.08%, 0.04-0.21, and 14.03-21.95 ºC, respectively) suggest deposition in semi-arid to semi-humid environment. Al_2O_3 stays dissolved in basic solutions above pH 9 and in acidic solutions below pH 4, indicating that the pH of the surrounding medium during Al_2O_3 deposition falls between these two ranges. The SiO_2 content decreases as pH rises. In the Rakb Formation, the correlation between SiO_2 and Al_2O_3 is weak (r = 0.33). Consequently, it appears that the Rakb Formation was formed in somewhat alkaline and comparatively warm conditions. An additional indication of this assumption is the abnormal P_2O_5 content (0.1-0.36%). Moreover, given that the Cl content (0.09-0.3%) is comparatively higher than the average of 0.001% provided by Turkian and Wedipohl (1961), warm climate and shallow restricted environment are both prevalent. The above statement indicate that there was a predominance of the semi-arid to semi-humid during the deposition of the Rakb Formation.

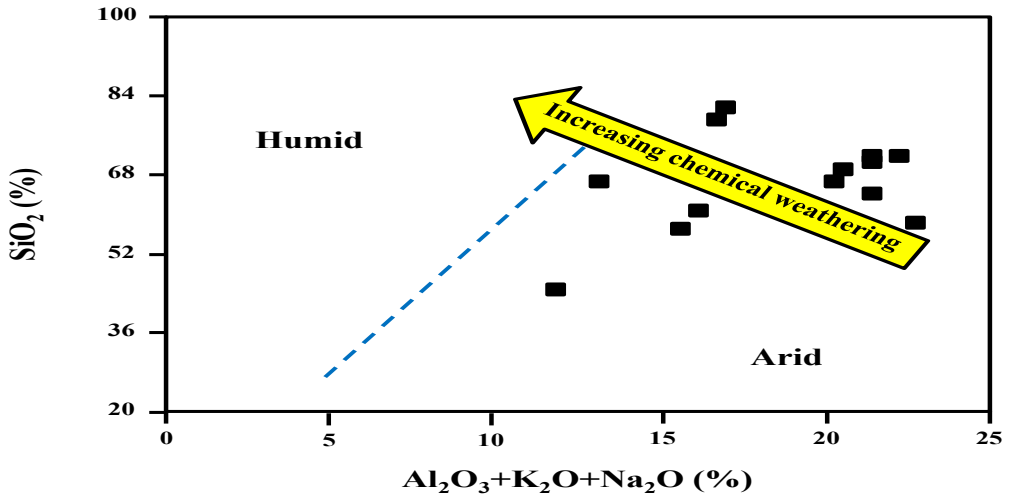

Fig. 21: Binary plot of $Al_2O_3+K_2O+Na_2O$ vs. SiO_2 showing the paleoclimate conditions in the source area (fields after Suttner and Dutta, 1986).

5.7. MATURITY

Cox *et al.,* (1995) reported that the maturity of sediments can be assessed using the index of compositional variability (ICV). This index is calculated as: $ICV = (Fe_2O_3+K_2O+Na_2O+CaO^*+MgO+MnO+TiO_2)/Al_2O_3$. High values (ICV>0.84) are indicative of immature sediments, whilst mature sediments display low values (ICV<0.84). The studied sediments are immature, according to the ICV values (0.97-1.33). The binary plot of CIA vs. ICV (Fig. 22) lends credence to this assumption.

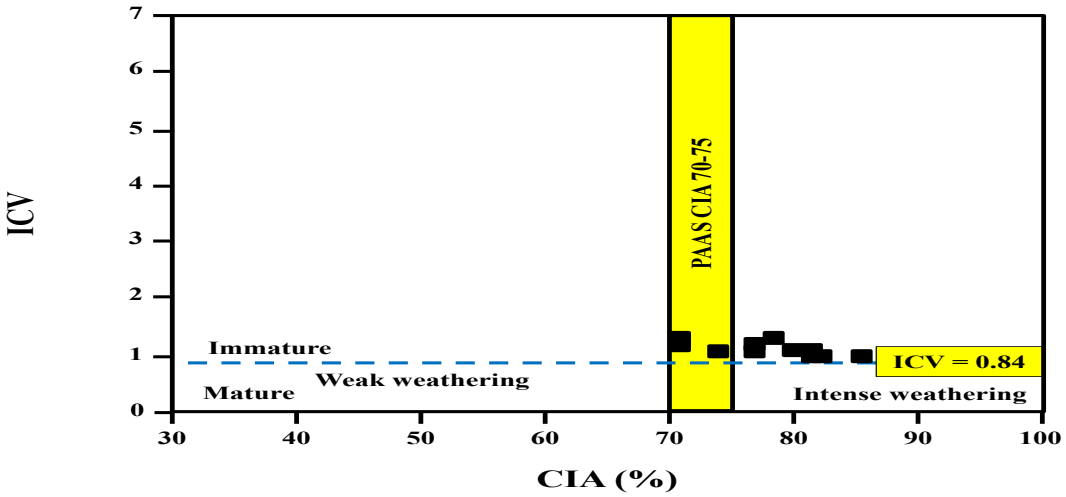

Fig. 22: Binary plot of CIA vs. ICV showing the maturity of the studied sediments (fields after Nesbitt and Young, 1982; Cox *et al.,* 1995).

5.8. PALEOPRODUCTIVITY

Numerous parameters, such as P/Al and P/Ti, can be used to assess paleoproductivity (Canfield, 1994; Yang *et al.,* 2022). High P/Al ratios indicate high paleoproductivity, while low paleoproductivity shows low ratios (Canfield, 1994). Furthermore, high paleoproductivity, medium paleoproductivity, and low paleoproductivity are often represented by P/Ti ratios of >0.79, 0.34-0.79, and <0.34, correspondingly (Yang *et al.,* 2022). The values of P/Al (0.004-0.02) and P/Ti (0.04-0.4) indicate that paleoproductivity ranged from low to high during deposition of the Rakb Formation.

5.9. PALEOTECTONIC SETTING

The four primary types of paleotectonic settings are: (1) Oceanic island arc (A); (2) Continental island arc (B); (3) Active continental margin (C); and (4) Passive margin (D). The Rakb Formation plotted in the continental margin fields in the plots of $Al_2O_3/(100\text{-}SiO_2)$ versus $Fe_2O_3/(100\text{-}SiO_2)$ (Fig. 23), SiO_2 versus K_2O/Na_2O (Fig. 24), and $SiO_2/20\text{-}K_2O+Na_2O\text{-}TiO_2+Fe_2O_3+MgO$ (Fig. 25).

6. CONCLUSION

In this work, major oxide data were used to assess the Rakb Formation in well C3-65, Sarir Field, Sirte Basin. The conclusions are as follows:

(1) Silica-rich argillaceous shale is the classification given to the Rakb Formation.

(2) Igneous (mafic, intermediate, and felsic rocks) and sedimentary (quartzose rocks) are among the many sources that contribute to the Rakb Formation.

(3) The shallow marine setting is the established depositional environment for the Rakb Formation (coastal facies). During the deposition, anoxic conditions were prevalent.

(4) Severe diagenesis has no discernible effect on the Rakb Formation.

(5) In the source area, the severity of paleoweathering ranged from moderate to high.

(6) Conditions during deposition were mostly semi-arid to semi-humid.

(7) The sediments are obviously immature.

(8) The range of paleoproductivity was low to high.

(9) The continental margin is the paleotectonic setting of the Rakb Formation.

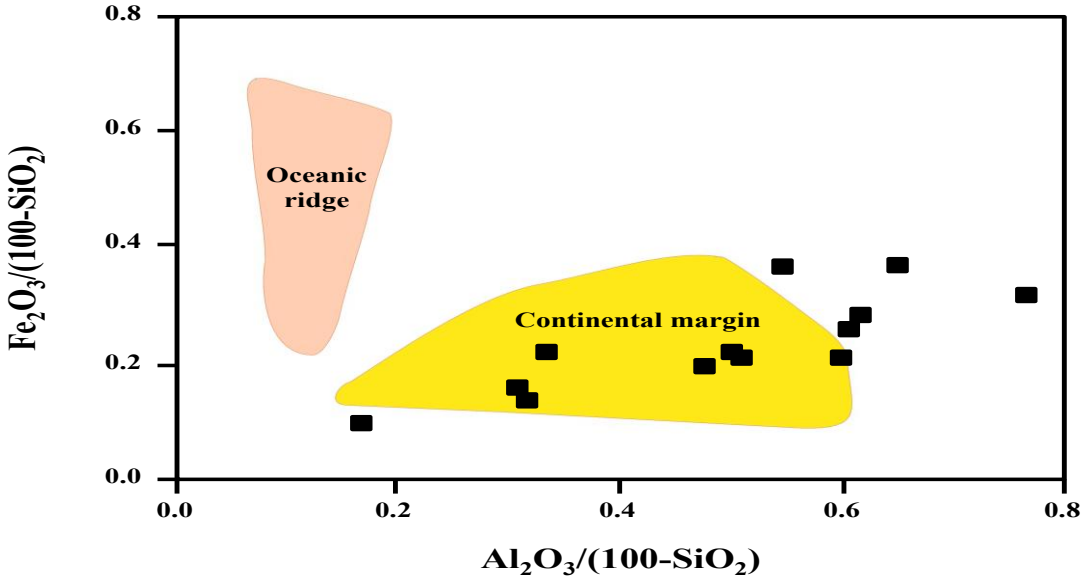

Fig. 23: Binary plot of $Al_2O_3/(100\text{-}SiO_2)$ vs. $Fe_2O_3/(100\text{-}SiO_2)$ showing the paleotectonic setting of the Rakb Formation (fields after He *et al.,* 2011).

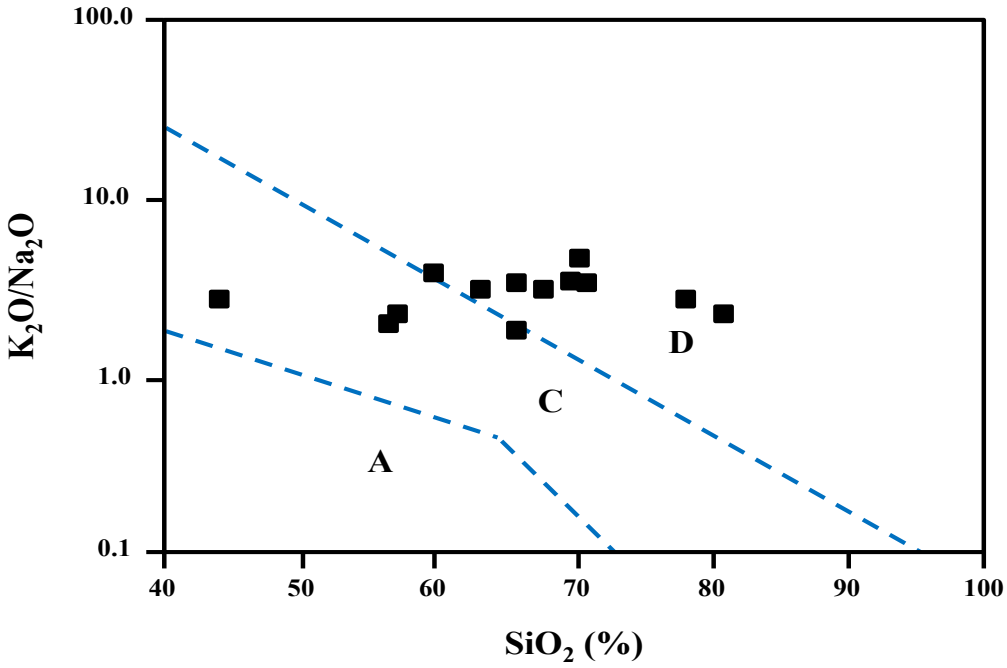

Fig. 24: Binary plot of SiO_2 vs. K_2O/Na_2O showing the paleotectonic setting of the Rakb Formation (fields after Roser and Korsch, 1986).

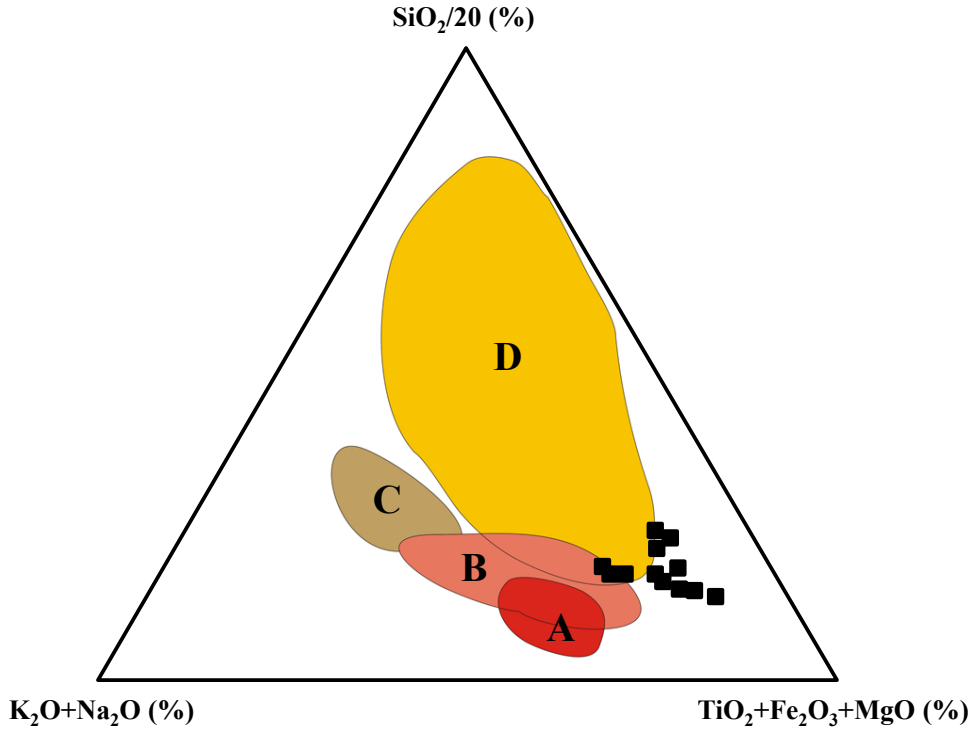

Fig. 25: Ternary plot of $SiO_2/20$-K_2O+Na_2O-$TiO_2+Fe_2O_3+MgO$ showing the paleotectonic setting of the Rakb Formation (fields after Kroonenberg, 1994).

ACKNOWLEDGMENT

The authors are grateful to Arabian Gulf Oil Company (AGOCO) for providing the samples used in this work.

7. REFERENCES

Aboglila, S., Grice, K., Trinajstic, K., Dawson, D. and Williford, K.H. (2010). Use of biomarker distributions and compound specific isotopes of carbon and hydrogen to delineate hydrocarbon characteristics in the east Sirte Basin (Libya). *Organic Geochemistry, 41*(12), 1249-1258.

Aboglila, S., Grice, K., Trinajstic, K., Snape, C. and Williford, K.H. (2011). The significance of 24-norcholestanes, 4-methylsteranes and dinosteranes in oils and source-rocks from east Sirte Basin (Libya). *Applied Geochemistry, 26*, 1694-1705.

Aboglila, S. and Elkhalgi, M. (2013). Organic geochemical evaluation of Cretaceous potential source rocks, east Sirte Basin, Libya. *International Journal of Geosciences, 4,* 700-710.

Barr, F.T. and Weegar, A.A. (1972). Stratigraphic nomenclature of the Sirte Basin, Libya. *Petroleum Exploration Society of Libya, Tripoli,* 179p.

Bellanca, A., Claps, M., Erba, E., Masetti, D., Neri, R., Premoli-Silva, I. and Venezia, F. (1996). Orbitally induced limestone/marlstone rhythms in the Albian-Cenomanian Cismon section (Venetian región, northern Italy): sedimentology, calcareous and siliceous plankton distribution, elemental and isotope geochemistry. *Palaeogeography, Palaeoclimatology, Palaeoecology, 126,* 227-260.

Canfield, D.E. (1994). Factors influencing organic carbon preservation in marine sediments. *Chemical Geology, 114,* 315-329.

Cao, Y., Songa, H., Algeo, T.J., Chu, D., Du, Y, Tian, L., Wang, Y. and Tong, J. (2019). Intensified chemical weathering during the Permian-Triassic transition recorded in terrestrial and marine successions. *Palaeogeography, Palaeoclimatology, Palaeoecology, 519,* 166-177.

Cox, R., Low, D.R. and Cullers, R.L. (1995). The influence of sediment recycling and basement composition on evolution of mudrock chemistry in the southwestern United States. *Geochimica et Cosmochimica Acta, 59,* 2919-2940.

Crook K.A.W. (1974). Lithogenesis and geotectonics: The significance of compositional variation in flysch arenites (greywackes). *Society for Sedimentary Geology Special Publication (SEPM),* 19, 304-310.

Cullers, R.L. (2000). The geochemistry of shales, siltstones, and sandstones of Pennsylvanian-Permian age, Colorado, USA: Implication for provenance and metamorphic studies. *Lithos, 51,* 181-203.

Cullers, R.L. and Podkovyrov, V.N. (2000). Geochemistry of the Mesoproterozoic Lakhanda shales in southeastern Yakutia, Russia: Implications for mineralogical and provenance control, and recycling. *Precambrian Research, 104,* 77-93.

Dhannoun, H.Y. and Al-Dlemi, A.M.S. (2013). The relation between Li, V, P_2O_5, and Al_2O_3 contents in marls and mudstones as indicators of environment of deposition. *Arabian Journal of Geosciences, 6,* 817-823.

EIA (U.S. Energy Information Administration, 2015). Technically recoverable shale oil and shale gas resources: Libya. *Technical Report,* 26p.

El-Mehdawi, A.D. (1998). *Odontochitina tabulata* sp. nov. A Late Santonian-Early Campanian dinoflagellate cyst from SE Sirte Basin, Libya. *Journal of Micropalaeontology, 17,* 173-178.

Fedo, C.M.; Nesbitt, H.W. and Young, G.M. (1995). Unraveling the effects of potassium metasomatism in sedimentary rocks and paleosols, with implications for paleoweathering conditions and provenance. *Geology, 23,* 921-924.

Gamero-Diaz, H., Miller, C. and Lewis, R. (2012). sCore: A classification scheme for organic mudstones based on bulk mineralogy. *American Association of Petroleum Geologists (AAPG), Search and Discovery Article #40951*.

Hallett, D. (2002). Petroleum geology of Libya. *Amsterdam, Elsevier Inc.,* 503p.

Hallett, D. and Clark-Lowes, D. (2016). Petroleum geology of Libya. *2nd edition, Amsterdam, Elsevier Inc.,* 404p.

Harnois, L. (1988). The CIW index: A new chemical index of weathering. *Sedimentary Geology, 55,* 319-322.

Hasterok, D., Gard, M., and Webb, J. (2018). On the radiogenic heat production of metamorphic, igneous, and sedimentary rocks. *Geoscience Frontiers, 9*(6), 1777-1794.

Hayashi, K., Fujisawa, H., Holland, H. and Ohmoto, H. (1997). Geochemistry of ~1.9 Ga sedimentary rocks from northeastern Labrador, Canada. *Geochimica et Cosmochimica Acta, 61*(19), 4115-4137.

He, C., Ji, L., Su, A., Wu, Y., Zhang, M., Zhou, S., Li, J., Hao, L. and Ma, Y. (2019). Source-rock evaluation and depositional environment of black shales in the Triassic Yanchang Formation, southern Ordos Basin, north-central China. *Journal of Petroleum Science and Engineering, 173,* 899-911.

He, J., Zhou, Y. and Li, H. (2011). Study on geochemical characteristics and depositional environment of Pengcuolin chert, Southern Tibet. *Journal of Geography and Geology, 3*(1), 178- 188.

Herron, M.M. (1988). Geochemical classification of terrigenous sandstone and shale from core and log data. *Journal of Sedimentary Petrology, 5*(8), 820-829.

Ibe, C.U. and Okon, E.E. (2021). Provenance and tectonic settings of the Eze‑Aku Sandstone (Turonian) in Awajir and adjoining areas, Southern Benue Trough, Nigeria: evidence from petrography and geochemistry. *Journal of Sedimentary Environments, 6,* 237-254.

Khan, D., Zijun, L., Qiu, L., Kuiyuan, L., Yongqiang, Y., Cong, N., Bin, L., Li, X. and Habulashenmu, Y. (2023). Mineralogical and geochemical characterization of lacustrine calcareous shale in Dongying Depression, Bohai Bay Basin: Implications for paleosalinity, paleoclimate, and paleoredox conditions. *Geochemistry, 83*(3), 125978.

Kronberg, B.I. and Nesbitt, H.W. (1981). Quantification of weathering, soil geochemistry and soil fertility. *Journal of Soil Science, 32*(3), 453-459.

Kroonenberg S.B. (1994). Effects of provenance, sorting and weathering on the geochemistry of fluvial sands from different tectonic and climatic environments. *29th International Geology Congress, Proceeding Book, Part A*, 69-81.

Liu, Z.H., Zhuang, X.G., Teng, G.E., Xie, X.M., Yin, L.M., Bian, L.Z., Feng, Q. and Algeo, T. (2015). The Lower Cambrian Niutitang Formation at Yangtiao (Guizhou, SW China): Organic matter enrichment, source rock potential, and hydrothermal influences. *Journal of Petroleum Geology, 38*, 411-432.

Lyons, T.W. and Severmann, S. (2006). A critical look at iron paleoredox proxies: New insights from modern euxinic marine basins. *Geochimica et Cosmochimica Acta, 70*(23), 5698-5722.

Machhour, L., Philip, J. and Oudin, J.L. (1994). Formation of laminate deposits in anaerobic-dysaerobic marine environments. *Marine Geology, 117*, 287-302.

McLennan, S.M., Hemming, S., McDaniel, D.K. and Hanson, G.N. (1993). Geochemical approaches to sedimentation, provenance, and tectonics. In Johnson, M.J. and Basu, A. (eds), Processes Controlling the Composition of Clastic Sediments. *Geological Society of America, Special Paper, 284*, 21-40.

Murphy, A.E., Sageman, B.B., Hollander, D.J., Lyons, T.W. and Brett, C.E. (2000). Black shale deposition and faunal overturn in the devonian appalachian basin: clastic starvation, seasonal water-column mixing, and efficient biolimiting nutrient recycling. *Paleoceanography, 15*(3), 280-291.

Naseem, S., Naseem, S. and Sheikh, S.A. (2005). Geochemical evaluation of depositional environment of Parh Limestone, Southern Pab Range, Balochistan, Pakistan. *SPE/PAPG Annual Technical Conference, Islamabad*, pp. 1-9.

Nesbitt, H.W. and Young, G.M. (1982). Early Proterozoic climates and plate motions inferred from major element chemistry of lutites. *Nature, 299*, 715-717.

Pettijohn, F.J. (1975). Sedimentary rocks. *2nd edition, Harper and Row Publishers*, 628 p.

Ratcliffe, K.T., Morton, A.C., Ritcey, D.H. and Evenchick, C.A. (2007). Whole-rock geochemistry and heavy mineral analysis as petroleum exploration tools in the Bowser and Sustut basins, British Columbia, Canada. *Bulletin of Canadian Petroleum Geology, 55*(4), 320-336.

Roser, B.P., and Korsch, R.J. (1986). Determination of tectonic setting of sandstone-mudstone suites using SiO_2 content and K_2O/Na_2O ratio. *Journal of Geology, 94*, 635-650.

Roser, B.P., and Korsch, R.J. (1988). Provenance signatures of sandstone- mudstone suites determined using discriminant function analysis of major-element data. *Chemical Geology, 67*, 119-139.

Roy, D.K. and Roser, B.P. (2013). Climatic control on the composition of Carboniferous–Permian Gondwana sediments, Khalaspir Basin, Bangladesh. *Gondwana Research, 23*(3), 1163-1171.

Ruxton, B.P. (1968). Measures of degree of chemical weathering of rocks. *The Journal of Geology, 76*(5), 515-527.

Saadawi, D.A., Ibrahim, A.M., AlSaad, H.A., Kamel, S.A. and Shalaby, A.M. (2023). Mineralogy and geochemistry of the Upper Cretaceous mudrocks, Wadi Feiran region, west-central Sinai, Egypt. *Iraqi Geological Journal, 56*(1F), 260-278.

Shaltami, O.R. (2024). Elemental geochemistry of the Awainat Wanin Formation in three selected areas, Murzuq Basin, SW Libya. *Global Scientific Journals (GSJ), 12*(2), 992-1016.

Shaltami, O.R., Algomati, A.E., and Geniber, O.A. (2024). Geochemistry of Al Mahruqah Formation: A case study of four areas in the northern Murzuq Basin, SW Libya. *Libyan Journal of Engineering Science and Technology (LJEST), 4*(1), 76-84.

Suttner, L.J. and Dutta, P.K. (1986). Alluvial sandstone composition and paleoclimate. Framework mineralogy. *Journal of Sedimentary Petrology, 56*, 326-345.

Taylor, S.R. and McLennan, S.M. (1985). The continental crust: Its composition and evolution. *Blackwell Scientific Publishers, Oxford*, 312p.

Wedepohl, K.H. (1978). Manganese: abundance in common sediments and sedimentary rocks. In Wedepohl, K.H. (eds), Handbook of Geochemistry. *Berlin, Springer, II/3*, 1-17.

Williams, J.J. (1972). Augila field, Libya: Depositional environment and diagenesis of sedimentary reservoir and description of igneous reservoir. In: Stratigraphic oil and gas fields; classification exploration methods and case histories (ed. R.E. King). *American Association of Petroleum Geologists (AAPG), 16*, 623-632.

Yang, M., Zuo, Y., Fu, X., Qiu, L., Li, W., Zhang, J., Zheng, Z. and Zhang, J. (2022). Paleoenvironment of the Lower Ordovician Meitan Formation in the Sichuan Basin and adjacent areas, China. *Minerals, 12*(1), 75.